



# Dispersion and orientation of montmorillonite in Nylon-6

Ilchgerel Dash<sup>1,\*</sup>, Robb Winter<sup>2</sup>, Ulziidelger Byambasuren<sup>1</sup>,  
Myagmarnaran Tsendenbazar<sup>3</sup>, Batbileg Sanjaa<sup>4</sup>

<sup>1</sup> Department of Chemical Engineering, School of Applied Sciences, Mongolian University of Sciences and Technology, Ulaanbaatar, Mongolia

<sup>2</sup> Department of Chemical and Biological Engineering, South Dakota School of Mines and Technology, Rapid city, United States of America

<sup>3</sup> Mechanical Maintenance for Factory of Erdenet Mining Industry, Erdenet, Mongolia

<sup>4</sup> Institute of Chemistry and Chemical Technology, Mongolian Academy of Science, Ulaanbaatar, Mongolia

\*Correspondence author. Email: [ilchgerel@must.edu.mn](mailto:ilchgerel@must.edu.mn)

## ABSTRACT

Incorporation of high aspect ratio nanoparticles can significantly increase mechanical properties such as elastic modulus and tensile strength, and the functionality of the obtained nanocomposites. In this work, organically modified montmorillonite (Cloisite 30B) is dispersed and simultaneously oriented in Nylon-6 matrix using a high shear thin film machine. Organically modified montmorillonite was loaded into Nylon-6 with percentage range of 1-5. Produced Nylon-6/montmorillonite nanocomposite material's properties were analyzed using TEM, XRD, and DSC apparatuses, MTS 810 machine as well as their gas permeability is tested. The characterization results showed that high degree of dispersion and orientation, tensile modulus was increased by approximately 66% compared to the pure Nylon-6, high degree of crystallinity; gas permeability was decreased by approximately 3.5 times than neat nylon-6. Additionally, we have recovered new  $\alpha_2$  crystal form in the nanocomposite materials with high degree of dispersed and oriented oMMT.

**Keywords:** Nylon-6, montmorillonite, dispersion, orientation, crystal.

## 1. INTRODUCTION

Over the last three decades, scientists and researchers have become strongly interested in modifying polymer mechanical and functional properties by incorporating nanoscale fillers with a low percentage to form polymer nanocomposites (PNCs). Incorporation of high aspect ratio nanoparticles (HARNPs) such as montmorillonite can significantly increase Young modulus [1-5] and tensile strength [3], crystal structure, gas permeability [6], and transparency [7] of the obtained nanocomposites (NCs) [8]. However, the improvements of the polymer nanocomposite properties are dependent on nanoparticles dispersion and orientation. The mechanical properties increment was low when the nanoparticles are dispersed poor while the mechanical properties was significantly increased when the dispersion was good. Lui et al. [9] and Cho et al. [10] reported that Young modulus was increased ~25% and ~40% of nylon-6 containing of 10% and 5% organically modified montmorillonite, respectively. Meanwhile, Ranade et al. [11] reported that

Young modulus decreased by 25% for 1wt% and only 8.3% increase for 5wt% of oMMT/N6 NCs when compared to neat N6.

Two dimensional NPs such as nanoclays promote  $\gamma$ -crystal forms [12, 13, 14]. For instance, XRD analysis shows  $\gamma_1$ - and  $\gamma_2$ -form crystals are at  $2\theta$  of  $10.7^\circ$  and  $21.3^\circ$  for N6/MMT NCs [15].

Anisotropic properties of high aspect ratio nanoparticles (HARNP) PNCs displayed very substantial physical effects in barrier properties. Generally, polymer nanoclay NCs show dramatic improvements of their barrier properties due to their tortuous gas diffusivity paths, known as Nielsen's theory [16, 17]. In order to enhance the barrier properties the clay platelets are exfoliated in the polymer matrix first, then the exfoliated clay platelets should be oriented.

## 2. EXPERIMENTAL

### 2.1. Materials

N6 was purchased from the BASF chemical company under the name of Ultramid B3K-Polyamide 6. Density and molecular weight of the N6 were 1183 g/cm<sup>3</sup> and 18,000 g/mol, respectively. Organically modified montmorillonite (oMMT), which is a natural MMT organically modified with a quaternary ammonium salt, was used as a reinforcing NP. The quaternary ammonium salt is comprised of methyl, bis-2-hydroxyethyl, tallow (~65% of C18, ~30% of C16, and ~5% of C14), and chloride. The oMMT with a commercial name of Cloisite 30B was supplied by Southern Clay Products Incorporation.

### 2.2. Experimental

#### 2.2.1. Twin-screw extruder production

In beginning of the work, N6 and oMMT were compounded together in a Coperion ZSK-25 co-rotating twin-screw extruder (TSE). The screws diameters and length were 25.0 mm and 1,200 mm, respectively. Barrel temperatures of the twin-screw extruder range from 220°C near the hopper to 240°C in die and screw speed was 100 rpm. The oMMT and N6 were fed together into the hopper of the twin-screw extruder by means of an automatic K-Tron Gravimetric feeder (Model: KML-KT20) in the desired amounts. The twin-screw extruder produced dispersed oMMT/N6 NC strands. These strands were immediately cooled in a water bath and continuously pelletized. The pellets were dried in vacuum oven at 80°C and -91 kPa for 24 hours. In addition, the oMMT powders were dried at 105°C and -91 kPa for 12 hours. The dried pellets and the oMMT were used to fabricate ribbons using HAAKE PolyLab single-screw extruder with a rotating drum. Barrel temperatures of the single-screw extruder ranged from 220°C near the hopper to 230°C at the die and screw speed was 60 rpm. The rotating drum surface temperature was ~38°C. In addition, neat N6 ribbons were also produced using the same method and conditions of oMMT/N6 NCs for reference characterization data.

#### 2.2.2. High shear thin film machine production

Concentrations of oMMT in N6 matrix were 0.5, 1, 3, and 5 wt%, and the NCs were coded as 0.5MZO, 1MZO, 3MZO, and 5MZO, respectively. "M" represents oMMT/N6 NCs while "Z" corresponds to low ~10,000 s<sup>-1</sup> (A), medium ~13,000 s<sup>-1</sup> (B), and high ~15,000 s<sup>-1</sup> (C) shear rates of dispersion, respectively. "O" indicates that the NCs were oriented. All orientations were achieved at the same shear rate of ~229 s<sup>-1</sup> for the oMMT/N6. The desired amount of the dried N6 pellets and oMMT powders were hand mixed in a plastic bag inside a fume hood, and kept in desiccator until needed. The dried materials are dispersed and simultaneously oriented using the high shear thin film machine (HSTFM).

#### 2.2.3. Characterization techniques

TEM investigations were performed using a JOEL JEM-2100 TEM microscope. A thin section approximately 100 nm in thickness was sectioned by ultra-microtome with a diamond knife for TEM analysis. An image processing program, ImageJ software was used for quantitative analysis of oMMT orientation within N6 matrix. Orientation angle of the oMMT clay platelets was measured manually relatively to the flow direction.

XRD patterns were registered in a Rigaku Ultima Plus diffractometric. The diffractometric is equipped with a curved graphite crystal filter. It was operated at 40 kV and 40 mA, in the 2-35° range, and at scan rate of 1 °/s, using Cu-K $\alpha$  radiation at room temperature. The films thicknesses were approximately 0.2 mm and supported on zero background sample plate as a sample holder.

Six to eight milligram samples were used for a DSC analysis. The samples were dried in a vacuum oven at 80°C and -91 kPa for 36 hours. A heating rate of 10°C/min was applied over a temperature range of 30-300°C. The analyses were run under helium atmosphere using a SDT Q600, TA instrument. Crystallinity percentages were calculated from ratio between enthalpy of actual samples melting to enthalpy of fully crystalline samples.

Tensile tests were performed using MTS 810 hydraulic system based on ASTM D 638. The dog bone shape specimens were made under category of type IV<sup>B</sup> size range. Five specimens were tested and properties were averaged. The tests were performed at two different speeds: the initial and secondary speed. The initial speed was 0.15 in/min (3.81mm/min) which is to ensure extensometer measurement for the tensile modulus. The secondary speed was 0.25 in/min (6.35 mm/min) to measure tensile strength and other properties. One inch gauge extensometer was used for measurement of the Young's modulus.

Neat N6 and oMMT/N6 NC films with ~200  $\mu$ m thicknesses were used to determine gas permeability. The film diameter of 22 mm was put on porous stainless steel support and fixed to the bottom of a high pressure cylinder. A 450 psi pressure was applied on the film side of the cylinder by nitrogen gas. The gas was gathered and volume was measured on other side (the support side) of the film for 10 hours.

## 3. RESULTS AND DISCUSSION

A high shear thin film machine was explicitly designed for dispersion and orientation of NPs within polymer matrix system. We have used HAAKE single screw extruder for melt and pump molten polymer and montmorillonite. Fig. 1 depicts digital images showing the dispersing behavior of oMMT within a N6 matrix which were fabricated by HAAKE single screw extruder and the high shear thin film machine.

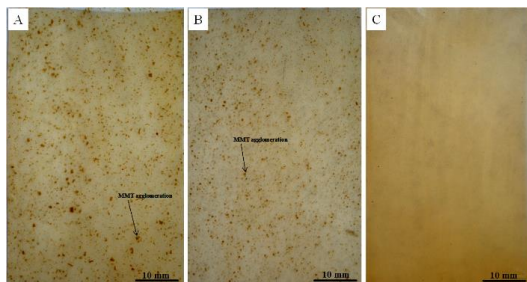


**Figure 1** Digital images of 5wt% oMMT/N6 NC films: (A) HAAKE single screw extruder production, (B) HSTFM mixer production with low shear rate of  $\sim 3000 \text{ s}^{-1}$ , (C) HSTFM production with maximum shear rate of  $\sim 15000 \text{ s}^{-1}$ .

The large brown dots in Fig. 1 are the oMMTs agglomerations while the lighter area is N6 matrix. Distributions of agglomeration are observed, the largest agglomeration dimensions are  $\sim 0.5 \text{ mm}$  wide and  $\sim 1.0 \text{ mm}$  long, as shown in Fig. 1A. This result shows that the HAAKE single screw extruder could not properly deagglomerate the oMMT agglomerations in N6 matrix. The HSTFM dispersion with low shear rate could also not adequately disperse oMMT in N6 matrix, as shown in Fig. 1B. However, the oMMTs agglomeration dimensions were decreased from  $\sim 0.5 \times 1.0 \text{ mm}$  to  $\sim 0.3 \times 0.5 \text{ mm}$ . HSTFM mixer with maximum shear rate produced NCs films with exfoliation of the oMMT in N6 matrix, as shown in Fig. 1C. The superior enhancement in degree of dispersion of oMMT in N6 matrix is contributed to high shear rate of  $\sim 15,000 \text{ s}^{-1}$ . TEM images of 5wt% of oMMT/N6 NCs are shown in Fig. 2-4.

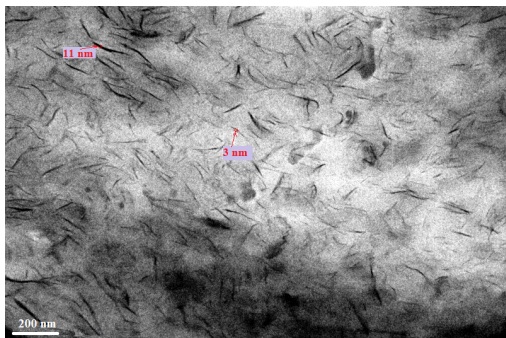


**Figure 2** TEM image of 5wt% oMMT/N6 at shear rates of  $10,000 \text{ s}^{-1}$  (5MA).

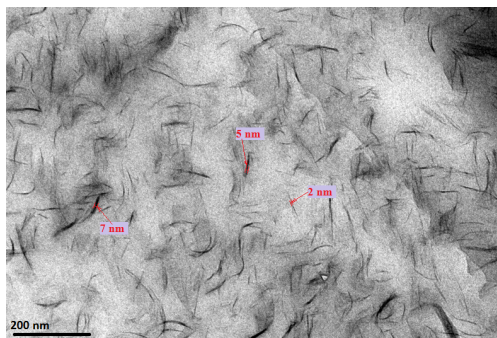


**Figure 3** TEM image of 5wt% oMMT/N6 at shear rates of  $13,000 \text{ s}^{-1}$  (5MB- MMT dispersed at medium shear rate of  $\sim 13,000 \text{ s}^{-1}$ ).

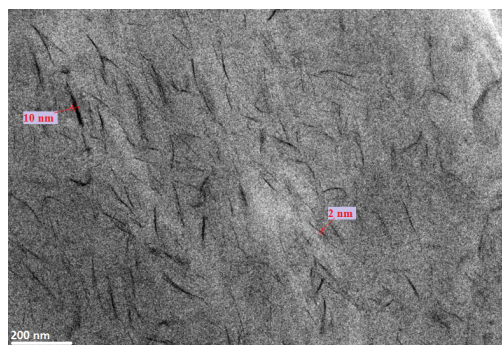


**Figure 4** TEM image of 5wt% oMMT/N6 at shear rates of  $15,000 \text{ s}^{-1}$  (5MC).

In these TEM images the black lines represent oMMT edges and light background represents the N6 matrix. The numbers within the images show the width of the agglomerates in nanometers. The TEM images show that improvement of oMMT de-agglomeration occurs with increasing of mixing shear rate from  $10,000$  to  $15,000 \text{ s}^{-1}$ . For instance, Fig. 2 shows some aggregates size  $\sim 11 \text{ nm}$  in thickness, which indicates medium degree of dispersion. These aggregates are a result of the lower medium dispersion shear rate of  $10,000 \text{ s}^{-1}$ . Whereas, Fig. 3 and 4 show a higher degree of dispersion was achieved than that shown in Figure 2. This result can be explained in that the HSTFM mixer with a high shear rate ( $\sim 15,000 \text{ s}^{-1}$ ) was applied efficient amount of energy to cause delamination of the MMT aggregates in the molten oMMT/N6 NCs system [8].

NCs of 5wt% oMMT/N6 were also dispersed using the twin-screw extruder, shown as in Figure 5.

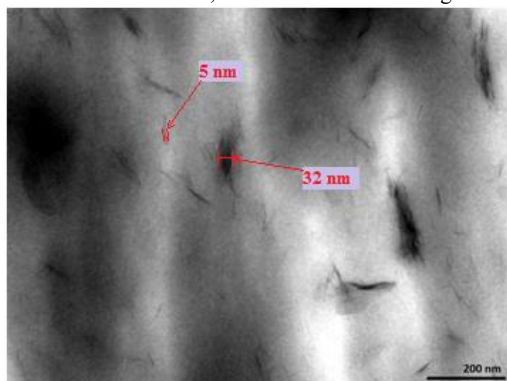
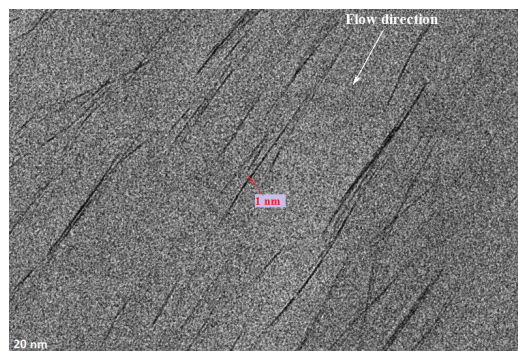


**Figure 5** TEM image of 5wt% oMMT/N6 NCs fabricated by twin-screw extruder (5M\_TSE).

Fig. 5 shows partial exfoliation of oMMTs agglomerations. Note that the large agglomerations having an average size of 30 nm in thickness are shown in Fig. 5. The reason for the poor dispersion oMMT in N6 is due to several factors. First, approximately only 15% of the total screw surface is used for creation of high shear rate of  $\sim 131 \text{ s}^{-1}$ . Additionally, the mixing residence time is short. As well, the oMMT and N6 pellets fed together into TSE hopper, which negatively affects the dispersion. Chavarria et al. [18] reported that they obtained poor dispersion because they feed NPs and polymer matrix together into the TSE hopper. The short mixing residence time indicates lower total energy was applied to the dispersing system which resulted in a lower degree of dispersion.

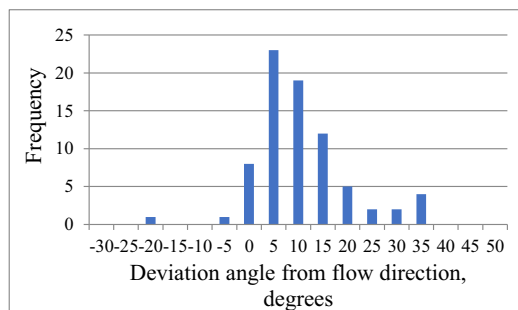
In order to obtain a high degree of NPs dispersion by TSE, residence time and screw rotation speed needed to be simultaneously increased. However, for a TSE, mixing residence time and screw rotation speed are inversely proportional to each other. One approach to increase the mixing residence time is to remix (recycle) the already extruded NC. Chavarria et al. [18] has reported that they obtained much better dispersion by re-mixing (re-extruding) the NCs 3 times via TSE when compared to re-mixing once. Additionally, Dennis et al. [19] reported that increasing the mixing residence time improved the dispersion of clay platelets.

Fig. 6 shows an image of dispersed and oriented 5wt% oMMT/N6 NCs (5MCO). The dispersion was achieved at the higher shear rate of  $15,000 \text{ s}^{-1}$  while the orientation was obtained at maximum shear rate of  $229 \text{ s}^{-1}$  in the HSTFM.



**Figure 6** TEM image of 5wt% oMMT orientation within N6 matrix, oriented using the HSTFM.

The ImageJ software was used for quantitative orientation analysis of orientated montmorillonites using the Fig. 6.



**Figure 7** Quantitative analysis of 5wt% oMMT orientation within N6, using Figure 6.

Result are presented in Fig. 7 which shows 81% of all oriented clay plates deviated  $-15^\circ$  and  $+15^\circ$  angle from the flow direction. The largest peak of frequency of oMMT orientation displayed at  $\sim 5^\circ$  angle from the flow direction. Based on Weon et al. report [20], using the orientation quantitative analysis, it is estimated that the maximum shear rate plane angle was  $\sim 5^\circ$  relative to flow direction.

XRD patterns of oMMT, N6, and oMMT/N6 NC films are shown in Fig. 8.

The XRD pattern of the pure oMMT displays a characteristic peak at  $4.8^\circ$  of  $2\theta$  angle with clay crystalline lamella size of  $>500 \text{ nm}$ . This indicates that clay platelets are regularly spaced with a  $1.8 \text{ nm}$  gap between each platelet. The neat N6 sample showed two characteristic peaks, at  $20.2$  and  $23.5^\circ$   $2\theta$  angle, which indicate  $\alpha_1$  and  $\alpha_2$  crystal forms, respectively.

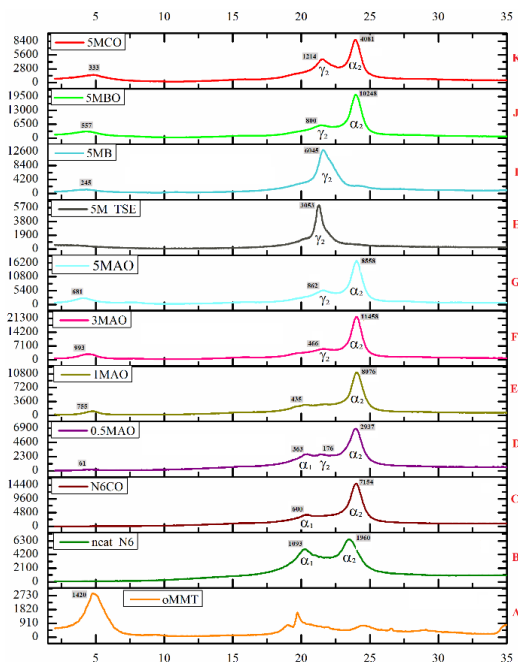


**Figure 8** XRD patterns of pure oMMT, neat N6, and oMMT/N6 films.

When the neat N6 is processed by the HSTFM at  $\sim 15,000$   $s^{-1}$  shear rate and oriented at maximum shear rate of  $229$   $s^{-1}$ , the  $\alpha_1$  crystal peak intensity shows a decrease from 1093 to 600 while  $\alpha_2$  intensity shows an increase from 1960 to 7154, as shown in Fig. 8C. The numbers on the gray background are the peak intensity heights in counts. The dispersed oMMT/N6 NC films show a significantly diminished characteristic peak of oMMT at  $\sim 4.8^\circ$   $2\theta$  angle. This implies that the gap between oMMT platelets has increased significantly and random.

There are two NC films which were subjected only to dispersion (8H and 8I), all others were dispersed and oriented. One of the two was 5wt% oMMT/N6 NC film (5M\_TSE) which is dispersed by twin-screw extruder, as shown in Fig. 8H. The other was also 5wt% oMMT/N6 NC film (5MB), is dispersed by the HSTFM at medium shear rate. These two films show a relatively small peak intensity at  $4.8^\circ$   $2\theta$  angle compared to the other samples dispersed and oriented by the HSTFM. This demonstrates that the orientation process of the HSTFM promotes polymer crystallinity and can be used to alter the polymer crystallinity of the NCs. Also  $\alpha_1$  and  $\alpha_2$  crystal forms are greatly reduced while  $\gamma_2$  is enhanced in only dispersed NCs.

As seen in Fig. 8, generally, the  $\alpha_2$  peaks intensity gradually increase with increasing oMMT loadings up to 3wt% oMMT then decreases for 5wt% oMMT. This can be explained in that the oMMT promotes the  $\alpha_2$  crystal form at lower oMMT loading, but hinders polymer chain mobility resulting in decreased crystallinity of the N6 at higher concentrations of the oMMT.

Polymer crystal form behavior of the dispersed NC film was totally different than the dispersed and oriented samples. The dispersed films showed only  $\gamma_2$  N6 crystal form while the dispersed and oriented films showed predominantly  $\alpha_2$  N6 crystal form and also  $\gamma_2$  N6 crystal form with small peak intensity. Many research articles [21, 22, 23] have reported that dispersed oMMT/N6 NC exhibits only  $\gamma_2$  crystal form. However, the  $\alpha_2$  crystal form with a very high intensity in oMMT/N6 NC has not been reported, possibly because a high degree of orientation of oMMT in a N6 matrix has not been obtained. It has been demonstrated in this work that the  $\alpha_2$  crystal form is promoted by a combination of the oMMT orientation and N6 chains orientation. Specifically, the HSTFM orientation process promotes the  $\alpha_2$  crystal form; this result was confirmed by the XRD pattern of HSTFM processed neat N6. This may be explained in that the  $\alpha_2$  crystal form is created from fully extended N6 chains with zig-zag conformation, while  $\gamma_2$  is created from twisted chains [24, 25].

Fig. 9 shows degree of crystallinity (DoC) from DSC analysis for neat N6 and oMMT/N6 NCs.

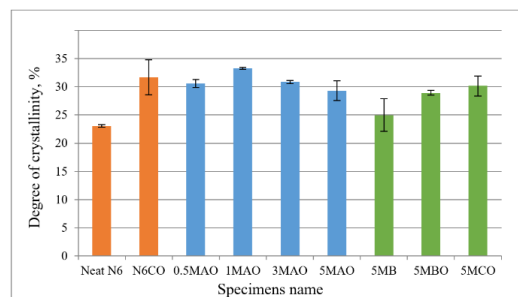


**Figure 9** Degree of crystallinity of neat N6 and oMMT/N6 NC films.

It can be seen from Fig. 9 that the DoC of the unprocessed neat N6 was  $\sim 23\%$ . Note that various authors have reported different DoC of neat N6 ranging from 18% to 27% [26, 22]. This value of 23% is lower than the value of  $\sim 32\%$  for neat N6CO which was processed by HSTFM. XRD results confirm that the unprocessed neat N6 film peak intensity was significantly lower than the neat N6CO NC film. The DoC of oMMT/N6 NC films was higher than unprocessed neat N6. Interestingly, N6 with 1wt% loading of oMMT exhibited the highest DoC of  $\sim 33\%$ . This suggests that there is an optimal concentration of the NPs in N6 matrix for nucleation and growth of N6 crystals. The DoC in NC films was decreased when the NPs loading was increased further. Karsli et al. [27] found a similar result at which the DoC decreased by  $\sim 18\%$  at 4wt% nanoparticles N6 NC compared to neat N6. They explained that the higher loading of the nanoparticles hinders the mobility of N6 chains [26, 27].

Tensile test results of neat N6 and the NC films are demonstrated in Fig. 10 and 11.

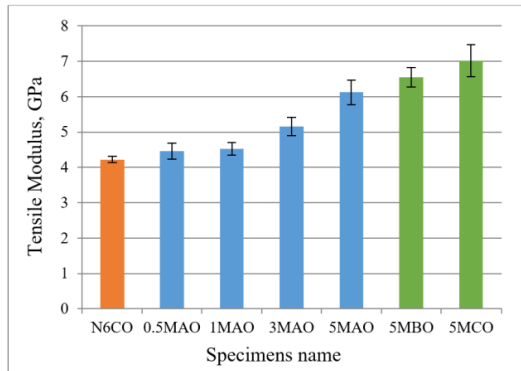


**Figure 10** Tensile modulus of neat N6 and its NC films.

Fig. 10 shows that the weight percent of oMMT and shear rate increase, the tensile moduli correspondingly increased. These results are in agreement with TEM and XRD results. The tensile modulus of 5MCO film is ~66% greater than the neat N6CO film. This significant increase in the tensile modulus can be attributed to the high degree of oMMTs dispersion and orientation in the N6, and also co-current orientation of the N6 chains. Additionally, segmental mobility of N6 chains is retarded near the oMMT surface due to favorable interfacial interaction between the N6 chains and oMMTs [28].

Fig. 11 shows tensile strength of the neat N6 and the NC films.

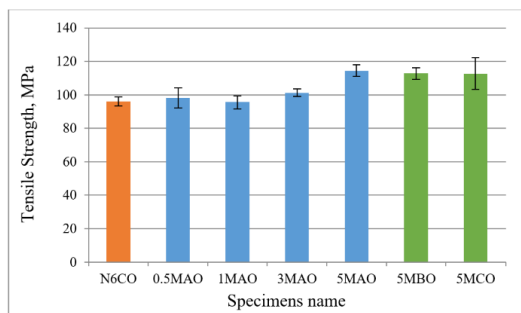


**Figure 11** Tensile strength of neat N6 and its NC films.

Tensile strength is not impacted at lower loadings of oMMT. At 5wt% oMMT/N6 NC films tensile strength increased by ~13% in comparison to the neat N6CO film. This can be attributed by relatively higher loading of oMMTs. Recall that 5MAO, 5MBO, and 5MCO were prepared at three different shear rates of  $10,000 \text{ s}^{-1}$ ,  $13,000 \text{ s}^{-1}$ , and  $15,000 \text{ s}^{-1}$ , respectively. Therefore, Fig. 11 shows that there was no significant tensile strength difference as a function of shear rate.

Fig. 12 shows the gas permeation amount through N6 and N6/oMMT NC films with various loading of oMMT.

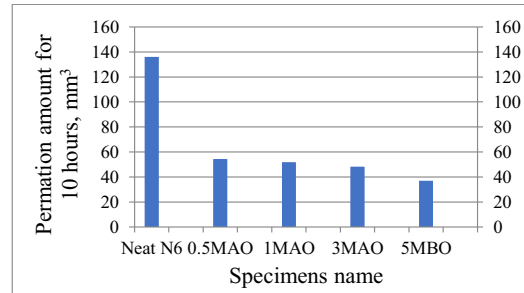


**Figure 12** Gas permeability of N6/oMMT NC films with various loading of oMMT.

The gas permeation amount is dramatically decreased when oMMTs are incorporated into N6 matrix. Fig. 12 indicates that neat N6 film gas permeation amount was  $\sim 136 \text{ mm}^3$  while 5MCO film was  $\sim 37 \text{ mm}^3$ , a decrease of approximately 3.5 times. Tsai et al. [29] reported that a gas permeation of 2 phr oMMT/N6 film decreased by  $\sim 4.4$  times in comparison to neat N6 film, which was prepared by in-situ polymerization followed by a hot pressing process. It is proposed that the high degree of dispersion and orientation of oMMT platelets is responsible for the improved barrier hindering gas diffusion through the film due to the increase in the tortuous path [30].

## CONCLUSION

Production of the high shear thin film machine with a various shear rate shows that moderate dispersion of organically modified montmorillonite in Nylon-6 matrix when applied medium shear rate while high degree of dispersion when applied maximum shear rate. TEM results revealed that high degree of orientation of the oMMT in Nylon-6 matrix, which can be obtained only after the exfoliation of the oMMT. Tensile test results of the obtained nanocomposite materials with high degree of dispersion and orientation showed that 5wt% of oMMT/N6 Young modulus was increased 66% in comparison with neat Nylon-6. The nanocomposite with high degree of dispersion possessed  $\gamma_2$  crystal form while  $\alpha_2$  crystal forms are recovered in dispersed and oriented oMMT/N6 nanocomposites. Gas permeability of oMMT/N6 nanocomposites with 5wt% loading was decreased by approximately 3.5 times compared to neat Nylon-6.

## ACKNOWLEDGMENTS

My sincere thanks and gratefully appreciation to the Chemical and Biological Engineering Department and Composite and Polymer Engineering Laboratory of South Dakota School of Mines and Technology for financial support and their faculty and staff for their support throughout my research and studies. Also I would like to acknowledge the Army Research Laboratory of USA for the funding support.

## REFERENCES

- [1] T. D. Fornes, D. L. Hunter, and D. R. Paul, Effect of sodium montmorillonite source on nylon 6/clay nanocomposites, *Polymer*, 45-7 (2004), pp. 2321-2331.  
<https://doi.org/10.1016/j.polymer.2004.01.061>
- [2] T. D. Fornes, P. J. Yoon, D. L. Hunter, H. Keskkula, and D. R. Paul, Effect of Organoclay structure on nylon 6 nanocomposite morphology and properties, *Polymer*, 43-22 (2002), pp. 5915-5933.  
[https://doi.org/10.1016/S0032-3861\(02\)00400-7](https://doi.org/10.1016/S0032-3861(02)00400-7)
- [3] T. X. Liu, I. Y. Phang, L. Shen, S. Y. Chow, and W. D. Zhang, Morphology and mechanical properties of multiwalled carbon nanotubes reinforced nylon-6 composites, *Macromolecules*, 37-19 (2004), pp. 7214-7222.
- [4] L. Shen, W. C. Tjiu, and T. X. Liu, Nanoindentation and morphological studies on injection-molded nylon-6 nanocomposites, *Polymer*, 46-25 (2005), pp. 11969-11977.  
<https://doi.org/10.1016/j.polymer.2005.10.006>
- [5] G. M. Magomedov, Z. L. Beslaneeva, A. C. Aigubova, and T. T. Ashat, Relaxation properties of nanocomposites based on polyamide 6 and organoclays, in *materials science forum*, 935 (2018), pp. 160-163.  
<https://doi.org/10.4028/www.scientific.net/MSF.935.160>
- [6] L. David, Jr. Statler, and R. K. Gupta, A finite element analysis of the influence of morphology on barrier properties of polymer-clay nanocomposites, in *COMSOL Conference, Boston, USA., (2007)*, pp. 7.
- [7] K. R. Atkinson, S. C. Hawkins, C. Huynh, C. Skourtis, J. Dai, M. Zhang, S. L. Fang, A. A. Zakhidov, S. B. Lee, A. E. Aliev, C. D. Williams, and R.H. Baughman, Multifunctional carbon nanotube yarns and transparent sheets: fabrication, properties, and applications, *Physica B-Condensed Matter*, 394-2 (2007), pp. 339-343.  
<https://doi.org/10.1016/j.physb.2006.12.061>
- [8] T. T. Zhu, C. H. Zhou, F. B. Kabwe, Q. Q. Wu, C. S. Li, and J. R. Zhang, Exfoliation of montmorillonite and related properties of clay/polymer nanocomposites, *Applied clay science*, 169 (2019), pp. 48-66.  
<https://doi.org/10.1016/j.clay.2018.12.006>
- [9] T. X. Liu, W. W. C. Tjiu, C. B. He, S. S. Na, and T. S. Chung, A processing-induced clay dispersion and its effect on the structure and properties of polyamide 6, *Polymer International*, 53-4 (2004), pp. 392-399.  
<https://doi.org/10.1002/pi.1359>
- [10] J. W. Cho, and D. R. Paul, Nylon 6 nanocomposites by melt compounding, *Polymer*, 42-3 (2001), pp. 1083-1094.  
[https://doi.org/10.1016/S0032-3861\(00\)00380-3](https://doi.org/10.1016/S0032-3861(00)00380-3)
- [11] A. Ranade, N. A. D'Souza, B. Gnade, and A. Dharia, Nylon-6 and montmorillonite-layered silicate (MLS) nanocomposites, *Journal of Plastic Film & Sheeting*, 19-4(2003), pp. 271-285.  
<https://doi.org/10.1177/8756087903042810>
- [12] C. Zhang, W. W. Tjiu, T. X. Liu, W. Y. Lui, I. Y. Phang, and W. D. Zhang, Dramatically enhanced mechanical performance of nylon-6 magnetic composites with nanostructured hybrid one-dimensional carbon nanotube-two-dimensional clay nanoplatelet heterostructures, *Journal of Physical Chemistry B*, 115-13 (2011), pp. 3392-3399.  
<https://doi.org/10.1021/jp112284k>
- [13] J. Gargalaka, R. A. A. Couto, V. R. L. Constantino, H. E. Toma, and K. Araki, Influence of the relative amounts of crystalline and amorphous phases on the mechanical properties of polyamide-6 nanocomposites, *Journal of Applied Polymer Science*, 125-4 (2012), pp. 3239-3249.  
<https://doi.org/10.1002/app.36509>
- [14] Y. Katoh, and M. Okamoto, Crystallization controlled by layered silicates in nylon 6-clay nanocomposite, *Polymer*, 50-19 (2009), pp. 4718-4726.  
<https://doi.org/10.1016/j.polymer.2009.07.019>
- [15] Y. Katoh, and M. Okamoto, Crystallization controlled by layered silicates in nylon 6-clay nanocomposite, *Polymer*, 50-19 (2009), pp. 4718-4726.  
<https://doi.org/10.1016/j.polymer.2009.07.019>
- [16] R. K. Bharadwaj, Modeling the barrier properties of polymer-layered silicate nanocomposites, *Macromolecules*, 34-26 (2001), pp. 9189-9192.  
<https://doi.org/10.1021/ma010780b>
- [17] C. S. Lu, and Y. W. Mai, Permeability modelling of polymer-layered silicate nanocomposites, *Composites Science and Technology*, 67-14 (2007), pp. 2895-2902.  
<https://doi.org/10.1016/j.compscitech.2007.05.008>
- [18] F. Chavarria, R. K. Shah, D. L. Hunter, and D. R. Paul, Effect of melt processing conditions on the morphology and properties of nylon 6 nanocomposites, *Polymer Engineering and Science*, 47-11 (2007), pp. 1847-1864.  
<https://doi.org/10.1002/pen.20894>
- [19] H. R. Dennis, D. L. Hunter, D. Chang, S. Kim, J. L. White, J. W. Cho, and D. R. Paul, Effect of melt processing conditions on the extent of exfoliation in organoclay-based nanocomposites, *Polymer*, 42-23 (2001), pp. 9513-9522.  
[https://doi.org/10.1016/S0032-3861\(01\)00473-6](https://doi.org/10.1016/S0032-3861(01)00473-6)
- [20] J. I. Weon, and H. J. Sue, Effects of clay orientation and aspect ratio on mechanical behavior of nylon-6 nanocomposite, *Polymer*, 46-17, (2005), pp. 6325-6334.  
<https://doi.org/10.1016/j.polymer.2005.05.094>
- [21] J. Gargalaka, R. A. A. Couto, V. R. L. Constantino, H.E. Toma, and K. Araki, Influence of the relative amounts of crystalline and amorphous phases on the mechanical properties of polyamide-6 nanocomposites, *Journal of Applied Polymer Science*, 125-4 (2012), pp. 3239-3249.  
<https://doi.org/10.1002/app.36509>

- [22] Y. Katoh, and M. Okamoto, Crystallization Controlled by layered silicates in nylon 6–clay nanocomposite, *Polymer*, 50-19 (2009), pp. 4718-4726.  
<https://doi.org/10.1016/j.polymer.2009.07.019>
- [23] H. E. Miltner, G. V. Assche, A. Posgay, B. Pukánszky and B.V. Mele, Restricted chain segment mobility in poly(amide) 6/clay nanocomposites evidenced by quasi isothermal crystallization, *Polymer*, 47-3 (2006), pp. 826-835.  
<https://doi.org/10.1016/j.polymer.2005.12.014>
- [24] A. W. Nienow, M. F. Edward, and N. Harnby, *Mixing in the process industries*. Butterworth-Heinemann, (1997), pp. 203.
- [25] C. W. Macosko, *Rheology: Principles, measurements, and applications*, WILEY-VCH. (1994) pp. 191.
- [26] J. A. Li, Z. P. Fang, L. F. Tong, A. J. Gu, and F. Liu, Polymorphism of nylon-6 in multiwalled carbon nanotubes/nylon-6 composites, *Journal of Polymer Science Part B-Polymer Physics*, 44-10, (2006), pp. 1499-1512.  
<https://doi.org/10.1002/polb.20808>
- [27] N. G. Karsli, and A. Aytac, Tensile and thermomechanical properties of short carbon fiber reinforced polyamide 6 composites, *Composites Part B: Engineering*, 51 (2013), pp. 270-275.  
<https://doi.org/10.1016/j.compositesb.2013.03.023>
- [28] E. Taghizadeh, G. Naderi, and M. R. Nouri, Effects of organoclay on the mechanical properties and microstructure of pa6/eco blend, *Polymer Testing*, 30-3, (2011), pp. 327-334.  
<https://doi.org/10.1016/j.polymertesting.2011.01.007>
- [29] T. Y. Tsai, W. H. Lin, Y. Y. Lin, Y. C. Hsu, U. Ray, Y. T. Lin, and M. J. Ou, Permeability property of nylon 6 nanocomposite membranes with various clay minerals, *Desalination*, 233-1 (2008), pp. 183-190.  
<https://doi.org/10.1016/j.desal.2007.09.041>
- [30] S. S. Ray, and M. Okamoto, Polymer/Layered silicate nanocomposites: a review from preparation to processing, *Progress in Polymer Science*, 28-11 (2003), pp. 1539-1641.  
<https://doi.org/10.1016/j.progpolymsci.2003.08.002>

**Open Access** This chapter is licensed under the terms of the Creative Commons Attribution-NonCommercial 4.0 International License (<http://creativecommons.org/licenses/by-nc/4.0/>), which permits any noncommercial use, sharing, adaptation, distribution and reproduction in any medium or format, as long as you give appropriate credit to the original author(s) and the source, provide a link to the Creative Commons license and indicate if changes were made.

The images or other third party material in this chapter are included in the chapter's Creative Commons license, unless indicated otherwise in a credit line to the material. If material is not included in the chapter's Creative Commons license and your intended use is not permitted by statutory regulation or exceeds the permitted use, you will need to obtain permission directly from the copyright holder.

